

# On a deterministic particle-FEM discretization to micro-macro models of dilute polymeric fluids

Xuelian Bao\*

*School of Mathematical Sciences, Laboratory of Mathematics and Complex Systems, MOE,  
Beijing Normal University, 100875 Beijing, China.*

*Research Center for Mathematics and Mathematics Education, Beijing Normal University at  
Zhuhai, 519087 Zhuhai, China.*

*Research Center for Mathematics, Beijing Normal University at Zhuhai, 519087 Zhuhai, China.*

Chun Liu† and Yiwei Wang‡

*Department of Applied Mathematics, Illinois Institute of Technology, Chicago, Illinois 60616,  
United States*

In this paper, we proposed a deterministic particle-FEM discretization to micro-macro models of dilute polymeric fluids, which combines a finite element discretization to macroscopic fluid dynamic equation with a variational particle scheme to the microscopic Fokker-Planck equation. The discretization is constructed by a discrete energetic variational approach, and preserves the microscopic variational structure in the semi-discrete level. Numerical examples demonstrate the accuracy and robustness of the proposed numerical scheme for some special external flows with a wide range of flow rates, compared to existing stochastic simulation methods and closure approximations.

## 1. Introduction

Complex fluids comprise a large class of soft materials, such as polymeric solutions, liquid crystals, ionic solutions, and fiber suspensions. These are fluids with complicated rheological phenomena, arising from different “elastic” effects, such as elasticity of deformable particles, interaction between charged ions and bulk elasticity endowed by polymer molecules.<sup>48</sup> Modeling and numerical simulations of complex fluids have been interesting problems for a couple of decades.<sup>8, 41, 43, 44</sup>

Models for complex fluids can be classified as pure macroscopic models<sup>37, 45, 64</sup> and micro-macro models.<sup>9, 43</sup> The macroscopic models utilize closed-form constitutive equations for the stress tensor  $\boldsymbol{\tau}$  to supplement the conservation of mass and momentum.<sup>37, 45, 64</sup> The micro-macro approach is to couple the macroscopic conservation laws with the microscopic kinetic theory.<sup>9, 43</sup> One of the simplest micro-macro models of complex fluids is the dumbbell model for a dilute polymeric fluid given

\*xlbao@bnu.edu.cn

†cliu124@iit.edu

‡ywang487@iit.edu, corresponding author

by<sup>47</sup>

$$\begin{cases} \rho(\mathbf{u}_t + \mathbf{u} \cdot \nabla \mathbf{u}) + \nabla p = \eta_s \Delta \mathbf{u} + \nabla \cdot \boldsymbol{\tau}, \\ \boldsymbol{\tau} = \lambda_p \mathbb{E}(\nabla_{\mathbf{q}} \Psi \otimes \mathbf{q}) = \lambda_p \int_{\mathbb{R}^d} f \nabla_{\mathbf{q}} \Psi \otimes \mathbf{q} d\mathbf{q}, \\ \nabla \cdot \mathbf{u} = 0, \\ f_t + \mathbf{u} \cdot \nabla f + \nabla_{\mathbf{q}} \cdot (\nabla \mathbf{u} \mathbf{q} f) = \frac{2}{\zeta} \nabla_{\mathbf{q}} \cdot (f \nabla_{\mathbf{q}} \Psi) + \frac{2k_B T}{\zeta} \Delta_{\mathbf{q}} f. \end{cases} \quad (1.1)$$

In this model, the macroscopic motion of the fluid is described by a Navier–Stokes equation with an elastic stress  $\boldsymbol{\tau}$  depending on the microscopic configuration of polymer chains, where  $\mathbf{u}$  denotes the fluid velocity field,  $p$  is the pressure,  $\rho$  is the density of the fluid, and  $\lambda_p$  is a parameter related to the polymer density. At the microscopic level, a polymer chain is modelled by a elastic dumbbell with two beads connected by a single spring. The molecular configuration is described by the end-to-end vector  $\mathbf{q} \in \mathbb{R}^d$  of the dumbbell and  $\Psi(\mathbf{q})$  is the spring potential. The interactions among polymer chains is neglected due to the dilute assumption. In the case that  $\Psi(\mathbf{q}) = \frac{H}{2} \|\mathbf{q}\|^2$  ( $H > 0$  is the elastic constant), the model is known as Hookean dumbbell model. While the case that  $\Psi(\mathbf{q}) = -\frac{H Q_0^2}{2} \ln(1 - (\frac{|\mathbf{q}|}{Q_0})^2)$  ( $Q_0$  is the maximum dumbbell extension) is known as the FENE (Finite Extensible Nonlinear Elastic) dumbbell model. The microscopic dynamics is described by a Fokker–Planck equation of the number density distribution function  $f(\mathbf{x}, \mathbf{q}, t)$  with a drift term depending on the macroscopic velocity field  $\mathbf{u}$ , where  $\zeta$  is related to the polymer relaxation time,  $k_B$  is the Boltzmann constant and  $T$  is the absolute temperature. Alternatively, the microscopic dynamics can also be described a stochastic differential equation (SDE), or a Langevin dynamics, given by<sup>12</sup>

$$d\mathbf{q}(\mathbf{x}, t) = (-\mathbf{u} \cdot \nabla \mathbf{q}(\mathbf{x}, t) + \nabla \mathbf{u} \mathbf{q}(\mathbf{x}, t) - 2\zeta^{-1} \nabla_{\mathbf{q}} \Psi(\mathbf{q}(\mathbf{x}, t))) dt + \sqrt{4k_B T \zeta^{-1}} d\mathbf{W}_t, \quad (1.2)$$

where  $d\mathbf{W}_t$  is the standard multidimensional white noise.

Although micro-macro models give an elegant description to the origin of the macroscopic stress tensor, it is a long lasting challenge to simulate micro-macro models directly. During the past decades, various computational techniques have been developed for various micro-macro models.<sup>22, 29, 31, 42, 54, 57</sup> There are mainly two approaches, the Langevin equation based stochastic simulation methods and direct simulation methods based on the Fokker–Planck equation.<sup>53</sup> The CONNFFESSIT (Calculation of Non-Newtonian Flow: Finite Elements and Stochastic Simulation Technique) algorithm, was the first Langevin equation based numerical method, which couples a finite element discretization to macroscopic flow with a numerical solver for the microscopic SDE (1.2).<sup>42, 57</sup> Along this direction, other stochastic approaches, the Lagrangian particle method (LPM),<sup>29</sup> the Brownian configuration field (BCF) method<sup>31</sup> were proposed in order to reduce the variance and the computational cost of the original CONNFFESSIT algorithm. Several extensions of these approaches and the corresponding numerical experiments have been ex-

tensively investigated in recent years.<sup>11,12,14,27,35,39,70</sup> Stochastic approaches have been the dominant part for the simulation of the micro-macro model. However, such stochastic approaches suffer from several shortcomings, including the high computational cost and the stochastic fluctuations. An alternative approach is the direct simulation of the equivalent Fokker–Planck equation in the configurational space. Examples include Galerkin spectral element technique<sup>15,38,52,63,66</sup> and the lattice Boltzmann technique.<sup>1,7</sup> As pointed out in Ref. 54, the computational cost of Fokker-Planck-based methods increases rapidly for simulations in strong flow (with highly localized distribution function) or involving high dimensional configuration space. Besides, there are a huge literature devoted to develop a macroscopic closure system, as an approximation to the original macro-micro model.<sup>21,25,33</sup>

There have been growing interests in solving Fokker-Planck equation by deterministic particle method.<sup>13,18,40,62,67</sup> The goal of the paper is to develop an efficient numerical method for the micro-macro model (1.1) by coupling a finite element discretization to the macroscopic flow with a deterministic particle discretization to the microscopic Fokker-Planck equation. The scheme is constructed by a discrete energetic variational approach,<sup>49,67</sup> which applies the particle approximation at the energy-dissipation law level first. Various numerical experiments have been performed to validate the new scheme via several benchmark problems. Despite its simplicity, the deterministic particle method is robust, accurate and able to catch certain complex behaviours of polymeric fluids. It is shown that numerical results obtained by our scheme are in excellent agreement with those from the former work. Moreover, our variational particle scheme is shown to be more efficient than using a stochastic approach, where a large ensemble of realisations of the stochastic process are needed. And contrary to stochastic simulations, this direct particle scheme gives solutions that are noise-free.

## 2. Energetic variational approach to the micro-macro model

In this section, we give a formal derivation to the micro-macro model for a dilute polymeric fluid by employing the energetic variational approach (EnVarA).

Starting with a prescribed energy-dissipation law and a kinematic (transport) relation, the framework of EnVarA derives the dynamics of a non-equilibrium system through two distinct variational processes: the Least Action Principle (LAP) and the Maximum Dissipation Principle (MDP).<sup>6,56</sup> This approach was developed from pioneering works of Rayleigh<sup>60</sup> and Onsager,<sup>55,56</sup> and has been successfully applied to build up many mathematical models in physics, chemical engineering and biology.<sup>26,48,68</sup> From a numerical perspective, the EnVarA formulation also provides a guide line to develop structure preserving numerical schemes for different systems.<sup>49</sup> For an isothermal and closed system, an energy-dissipation law is often given by

$$\frac{d}{dt} E^{\text{total}}(t) = -\Delta(t) \leq 0, \quad (2.1)$$

which comes from the first and second laws of thermodynamics.<sup>23,26</sup> Here  $E^{\text{total}}$  is the total energy, which is the sum of the Helmholtz free energy  $\mathcal{F}$  and the kinetic energy  $\mathcal{K}$ ;  $\Delta(t)$  stands for the rate of energy dissipation, which equals to the entropy production in this case. The LAP states that, the dynamics of the Hamiltonian part of the system can be determined by taking variation of the action functional  $\mathcal{A}(\mathbf{x}) = \int_0^T \mathcal{K} - \mathcal{F} dt$  with respect to  $\mathbf{x}$  (the trajectory in Lagrangian coordinates),<sup>2,26</sup> which derives the conservative force

$$\delta \mathcal{A} = \int_0^T \int_{\Omega^t} (\text{force}_{\text{iner}} - \text{force}_{\text{conv}}) \cdot \delta \mathbf{x} d\mathbf{x} dt, \quad (2.2)$$

where  $\Omega^t$  is the physical domain at time  $t$ . For a dissipative system ( $\Delta(t) \geq 0$ ), the dissipative force can be obtained by minimizing the Onsager dissipation functional  $\mathcal{D} = \frac{1}{2} \Delta(t)$  with respect to the "rate"  $\mathbf{x}_t$  in the linear response regime, i.e.,

$$\delta \mathcal{D} = \int_{\Omega(t)} \text{force}_{\text{diss}} \cdot \delta \mathbf{x}_t d\mathbf{x}. \quad (2.3)$$

This principle is known as Onsager's MDP.<sup>26,55,56</sup> Consequently, the force balance condition (Newton's second law, in which the inertial force plays a role of  $ma$ ) results in

$$\frac{\delta \mathcal{A}}{\delta \mathbf{x}} = \frac{\delta \mathcal{D}}{\delta \mathbf{x}_t}, \quad (2.4)$$

which is the dynamics of the system.

In the framework of EnVarA, the micro-macro system can be modeled through the energy-dissipation law

$$\begin{aligned} \frac{d}{dt} \int_{\Omega} \left( \frac{1}{2} \rho |\mathbf{u}|^2 + \lambda_p \int_{\mathbb{R}^d} k_B T f \ln f + \Psi f d\mathbf{q} \right) d\mathbf{x} \\ = - \int_{\Omega} \left( \eta_s |\nabla \mathbf{u}|^2 + \int_{\mathbb{R}^d} \frac{\lambda_p \zeta}{2} f |\mathbf{V} - \nabla \mathbf{u} \mathbf{q}|^2 d\mathbf{q} \right) d\mathbf{x}, \end{aligned} \quad (2.5)$$

where  $\mathbf{V}$  is the efficient microscopic velocity, the constant  $\rho$  is the density of the fluid,  $\lambda_p$  is a constant that represents the polymer density,  $k_B$  is the Boltzmann constant,  $T$  is the absolute temperature,  $\eta_s$  is the solvent viscosity, the constant  $\zeta$  is related to the polymer relaxation time,  $\Psi = \Psi(\mathbf{q})$  is the microscopic elastic potential of the polymer molecules, and  $f(\mathbf{x}, \mathbf{q}, t)$  is the number density distribution function. For the Hookean and the FENE models, the elastic potential  $\Psi(\mathbf{q})$  is given by

$$\Psi(\mathbf{q}) = \frac{1}{2} H |\mathbf{q}|^2,$$

and

$$\Psi(\mathbf{q}) = -\frac{H Q_0^2}{2} \ln \left( 1 - \left( \frac{|\mathbf{q}|}{Q_0} \right)^2 \right),$$

respectively, where  $H > 0$  is the elastic constant,  $Q_0$  is the maximum dumbbell extension in FENE model.

To compute the variations, one needs to introduce Lagrangian descriptions in both micro- and macro- scales. Let  $\mathbf{x}(\mathbf{X}, t)$  be the flow map at the physical space and  $\mathbf{q}(\mathbf{X}, \mathbf{Q}, t)$  be the flow map at the configuration space, where  $\mathbf{X}$  and  $\mathbf{Q}$  are Lagrangian coordinates in physical and configurational space respectively. For given flow maps  $\mathbf{x}(\mathbf{X}, t)$  and  $\mathbf{q}(\mathbf{X}, \mathbf{Q}, t)$ , the corresponding macroscopic velocity  $\mathbf{u}$  and the microscopic velocity  $\mathbf{V}$  satisfy

$$\mathbf{u}(\mathbf{X}, t) = \mathbf{x}_t(\mathbf{X}, t), \quad \mathbf{V}(\mathbf{X}, \mathbf{Q}, t) = \mathbf{q}_t(\mathbf{X}, \mathbf{Q}, t). \quad (2.6)$$

Moreover, one can define the deformation tensor associated with the flow map  $\mathbf{x}(\mathbf{X}, t)$  by

$$\tilde{\mathbf{F}}(\mathbf{x}(\mathbf{X}, t), t) = \mathbf{F}(\mathbf{X}, t) = \nabla_{\mathbf{X}} \mathbf{x}(\mathbf{X}, t). \quad (2.7)$$

Without ambiguity, in this paper, we will not distinguish  $\mathbf{F}$  and  $\tilde{\mathbf{F}}$ . Obviously,  $\mathbf{F}$  carries all the transport information of configurations in the system<sup>46</sup> and satisfies the transport equation in Eulerian coordinates<sup>47</sup>

$$\mathbf{F}_t + \mathbf{u} \cdot \nabla \mathbf{F} = \nabla \mathbf{u} \mathbf{F}.$$

Due to the conservation of mass, the density distribution function  $f(\mathbf{x}, \mathbf{q}, t)$  satisfies

$$\frac{d}{dt} \int_{\Omega} \int_{\mathbb{R}^d} f(\mathbf{x}, \mathbf{q}, t) d\mathbf{q} d\mathbf{x} = 0, \quad (2.8)$$

which can be written as

$$\partial_t f + \nabla \cdot (f \mathbf{u}) + \nabla_{\mathbf{q}} \cdot (f \mathbf{V}) = 0 \quad (2.9)$$

in Eulerian coordinates. The second term in the dissipation in (2.5) can be understood through the Cauchy-Born rule,  $\mathbf{q} = \mathbf{F} \mathbf{Q}$  at the macroscopic scale. Indeed, a direct computation results in

$$\tilde{\mathbf{V}} = \frac{d}{dt} (\mathbf{F} \mathbf{Q}) = \left( \frac{d}{dt} \mathbf{F} \right) \mathbf{Q} = (\nabla \mathbf{u} \mathbf{F}) \mathbf{Q} = \nabla \mathbf{u} \mathbf{q},$$

which is the induced velocity in the microscopic scale.

Now we are ready to derive the dynamics of the system. First, we look at the dynamics at the macroscopic scale. Due to the "separation of scale",<sup>26</sup> the second term on the right hand side of the dissipation (2.5) vanishes when deriving the macroscopic force balance. Since  $\det F = 1$ , the action functional can be written as

$$\mathcal{A}(\mathbf{x}) = \int_0^T \int_{\Omega_0} \left[ \frac{1}{2} \rho_0 |\mathbf{x}_t|^2 - \lambda_p \int_{\mathbb{R}^d} k_B T f_0 \ln f_0 + \Psi(\mathbf{F} \mathbf{Q}) f_0 d\mathbf{Q} \right] d\mathbf{X} dt \quad (2.10)$$

in Lagrangian coordinates. By applying the LAP, i.e., taking variation of  $\mathcal{A}(\mathbf{x})$  with respect to  $\mathbf{x}$ , we get

$$\frac{\delta \mathcal{A}}{\delta \mathbf{x}} = -\rho \mathbf{x}_{tt} + \lambda_p \nabla \cdot \left( \int_{\mathbb{R}^d} f \nabla_{\mathbf{q}} \Psi \otimes \mathbf{q} d\mathbf{q} \right). \quad (2.11)$$

For the dissipation part, the MDP, i.e., taking variation of  $\mathcal{D}$  with respect to  $\mathbf{x}_t$ , leads to

$$\frac{\delta \mathcal{D}}{\delta \mathbf{x}_t} = -\eta_s \Delta \mathbf{u} + \nabla p, \quad (2.12)$$

where  $p$  is the Lagrangian multiplier for the incompressible condition  $\nabla \cdot \mathbf{u} = 0$ . Hence, the macroscopic force balance results in the momentum equation

$$\rho(\mathbf{u}_t + \mathbf{u} \cdot \nabla \mathbf{u}) + \nabla p = \eta_s \Delta \mathbf{u} + \nabla \cdot \boldsymbol{\tau}, \quad (2.13)$$

where

$$\boldsymbol{\tau} = \lambda_p \int_{\mathbb{R}^d} f \nabla_{\mathbf{q}} \Psi \otimes \mathbf{q} d\mathbf{q} \quad (2.14)$$

is the induced stress from the configuration space, representing the microscopic contributions to the macroscopic level. Here,  $\otimes$  denotes a tensor product and  $\mathbf{u} \otimes \mathbf{v}$  is a matrix  $(u_i v_j)$  for two vectors  $\mathbf{u}$  and  $\mathbf{v}$ .

On the microscopic scale, by taking variations with respect to  $\mathbf{q}(\mathbf{X}, \mathbf{Q}, t)$  and  $V(\mathbf{X}, \mathbf{Q}, t)$ , we obtain

$$\frac{\zeta}{2}(V - \nabla \mathbf{u} \mathbf{q}) = -\nabla_{\mathbf{q}}(k_B T \ln f + 1 + \Psi).$$

Then combining with Eq. (2.9), we get the equation on the microscopic scale:

$$f_t + \nabla \cdot (\mathbf{u} f) + \nabla_{\mathbf{q}} \cdot (\nabla \mathbf{u} \mathbf{q} f) = \frac{2}{\zeta} \nabla_{\mathbf{q}} \cdot (f \nabla_{\mathbf{q}} \Psi) + \frac{2k_B T}{\zeta} \Delta_{\mathbf{q}} f. \quad (2.15)$$

And thus, the final coupled system reads as follows,

$$\begin{cases} \rho(\mathbf{u}_t + \mathbf{u} \cdot \nabla \mathbf{u}) + \nabla p = \eta_s \Delta \mathbf{u} + \nabla \cdot \boldsymbol{\tau}, \\ \boldsymbol{\tau} = \lambda_p \int_{\mathbb{R}^d} f \nabla_{\mathbf{q}} \Psi \otimes \mathbf{q} d\mathbf{q}, \\ \nabla \cdot \mathbf{u} = 0, \\ f_t + \nabla \cdot (\mathbf{u} f) + \nabla_{\mathbf{q}} \cdot (\nabla \mathbf{u} \mathbf{q} f) = \frac{2}{\zeta} \nabla_{\mathbf{q}} \cdot (f \nabla_{\mathbf{q}} \Psi) + \frac{2k_B T}{\zeta} \Delta_{\mathbf{q}} f, \end{cases} \quad (2.16)$$

subject to a suitable boundary condition. For the sake of simplicity, in this paper, we consider Dirichlet boundary conditions for the velocity and non-flux boundary condition for  $f(\mathbf{x}, \mathbf{q}, t)$  with respect to  $\mathbf{x}$ .

### 3. Numerical Methods

In this section, we propose a numerical scheme to solve the micro-macro model by combining a finite element discretization to macroscopic fluid dynamic equation<sup>4, 5, 16</sup> with a deterministic particle method for the microscopic Fokker-Planck equation.<sup>67</sup>

To preserve the variational structure after a particle discretization, we first derive the micro-macro system with a deterministic particle approximation in the configurational space by a discrete energetic variational approach.<sup>49</sup> The discrete energetic

variation approach is based on the "Approximation-then-Variation" method. The particle-based approximation of the density is performed first and then the approximated density is used in the discrete energy variational procedure. Hence, the derived ordinary differential equations of particles preserve the variational structure at the particle level.<sup>67</sup>

For simplicity, we assume that

$$\int_{\mathbb{R}^d} f(\mathbf{x}, \mathbf{q}, t) d\mathbf{q} = 1, \quad (3.1)$$

which means that the number density of polymer chains is spatially homogeneous. Thus, for fixed  $\mathbf{x}$ ,  $f(\mathbf{x}, \mathbf{q}, t)$  can be approximated by

$$f(\mathbf{x}, \mathbf{q}, t) \approx f_N(\mathbf{x}, \mathbf{q}, t) = \sum_{i=1}^N \omega_i(\mathbf{x}, t) \delta(\mathbf{q} - \mathbf{q}_i(\mathbf{x}, t)), \quad \forall \mathbf{x} \quad (3.2)$$

with a particle approximation at the microscopic level. Here  $N$  is the number of particles at  $\mathbf{x}$  and time  $t$ ,  $\{\mathbf{q}_i(\mathbf{x}, t)\}_{i=1}^N$  is a set of representative particles at  $\mathbf{x}$  at time  $t$ ,  $\omega_i(\mathbf{x}, t)$  is the weight of the corresponding particle satisfying  $\sum_i \omega_i(\mathbf{x}, t) = 1$ . In the current work, we fix  $\omega_i(\mathbf{x}, t) = \frac{1}{N}$ , i.e., all particles are equally weighted.

**Remark 3.1.**  $\{\mathbf{q}_i(\mathbf{x}, t)\}_{i=1}^N$  can be viewed as representative particles that represent information of the number density distribution  $f(\mathbf{x}, \mathbf{q}, t)$  at  $\mathbf{x}$ . Since only  $\mathbf{q}_i(\mathbf{x}, t)$  needs to be computed at each time-step, the computational cost can be largely reduced. It is more like an Eulerian approach, rather than a Lagrangian approach.

Substitute the approximation (3.2) into the continuous energy-dissipation law (2.5), we can obtain a discrete energy-dissipation law in terms of  $\mathbf{q}_i(\mathbf{x}, t)$  and the macroscopic flow. However, from a computational point of view, the term  $\ln f_N(\mathbf{x}, \mathbf{q}, t)$  can not be defined in a proper way. To deal with this issue, we introduce a kernel regularization, i.e., replacing  $\ln f_N$  by  $\ln(K_h * f_N)$ , where  $K_h$  is a kernel function and

$$K_h * f_N(\cdot, \mathbf{q}, \cdot) = \int K_h(\mathbf{q} - \mathbf{p}) f_N(\cdot, \mathbf{p}, \cdot) d\mathbf{p} = \frac{1}{N} \sum_{j=1}^N K_h(\mathbf{q} - \mathbf{q}_j(\mathbf{x}, t)).$$

A typical choice of  $K_h$  is the Gaussian kernel, given by

$$K_h(\mathbf{q}_1, \mathbf{q}_2) = \frac{1}{(\sqrt{2\pi}h_p)^d} \exp\left(-\frac{|\mathbf{q}_1 - \mathbf{q}_2|^2}{2h_p^2}\right).$$

Here  $h_p$  is the bandwidth which controls the inter-particle distances and  $d$  is the dimension of the space. We take  $h_p$  as a constant for simplicity. The value of  $h_p$  will affect the numerical results. We'll discuss the choice of  $h_p$  in the next section.

Within the kernel regularization, the discrete energy can be written as

$$\mathcal{F}_h[\{\mathbf{q}_i\}_{i=1}^N, \mathbf{x}] = \int_{\Omega} \frac{1}{2} \rho |\mathbf{u}|^2 + \lambda_p \frac{1}{N} \sum_{i=1}^N \left[ k_B T \ln \left( \frac{1}{N} \sum_{j=1}^N K_h(\mathbf{q}_i - \mathbf{q}_j) \right) + \Psi(\mathbf{q}_i) \right] d\mathbf{x}, \quad (3.3)$$

and the discrete dissipation is

$$-2\mathcal{D}_h[\{\mathbf{q}_i\}_{i=1}^N, \{\dot{\mathbf{q}}_i\}_{i=1}^N, \mathbf{x}, \mathbf{u}] = -\int_{\Omega} \eta_s |\nabla \mathbf{u}|^2 + \frac{\lambda_p \zeta}{2} \frac{1}{N} \sum_{i=1}^N |\dot{\mathbf{q}}_i - \nabla \mathbf{u} \mathbf{q}_i|^2 d\mathbf{x}, \quad (3.4)$$

where  $\dot{\mathbf{q}}_i = \partial_t \mathbf{q}_i + \mathbf{u} \cdot \nabla \mathbf{q}_i$  is the material derivative of  $\mathbf{q}_i$ .

The differential equations of  $\mathbf{q}_i$  can be derived via the discrete energetic variational approach,<sup>49</sup> i.e., performing the EnVarA in terms of  $\mathbf{q}_i$  and  $\dot{\mathbf{q}}_i$ , which leads to

$$\frac{\delta \mathcal{D}_h}{\delta \dot{\mathbf{q}}_i} = -\frac{\delta \mathcal{F}_h}{\delta \mathbf{q}_i}.$$

By direct computation we get the equation for  $\forall \mathbf{x}$

$$\begin{aligned} & \partial_t \mathbf{q}_i + \mathbf{u} \cdot \nabla \mathbf{q}_i - (\nabla \mathbf{u}) \mathbf{q}_i \\ &= -\frac{2}{\zeta} \left[ k_B T \left( \frac{\sum_{j=1}^N \nabla_{\mathbf{q}_i} K_h(\mathbf{q}_i, \mathbf{q}_j)}{\sum_{j=1}^N K_h(\mathbf{q}_i, \mathbf{q}_j)} + \sum_{k=1}^N \frac{\nabla_{\mathbf{q}_i} K_h(\mathbf{q}_k, \mathbf{q}_i)}{\sum_{j=1}^N K_h(\mathbf{q}_k, \mathbf{q}_j)} \right) + \nabla_{\mathbf{q}_i} \Psi(\mathbf{q}_i) \right]. \end{aligned} \quad (3.5)$$

Here we denote  $K_h(\mathbf{q}_i - \mathbf{q}_j)$  by  $K_h(\mathbf{q}_i, \mathbf{q}_j)$  for convenience. As an advantage of the ‘‘approximation-then-variation’’ approach, it can be noticed that Eq. (3.5) is a gradient flow with respect to  $\{\mathbf{q}_i\}$  in absence of the flow, i.e.  $\mathbf{u} = 0$  at  $\forall \mathbf{x}$ .

The variational procedure for the macroscopic flow is almost the same to that in the continuous case, shown in section 2. The final micro-macro system with particle approximation is given by

$$\begin{cases} \rho(\mathbf{u}_t + \mathbf{u} \cdot \nabla \mathbf{u}) + \nabla p = \eta_s \Delta \mathbf{u} + \nabla \cdot \boldsymbol{\tau}, \\ \boldsymbol{\tau}(\mathbf{x}, t) = \lambda_p \frac{1}{N} \sum_{i=1}^N \nabla_{\mathbf{q}} \Psi(\mathbf{q}_i(\mathbf{x}, t)) \otimes \mathbf{q}_i(\mathbf{x}, t), \\ \nabla \cdot \mathbf{u} = 0, \end{cases} \quad (3.6)$$

where  $\mathbf{q}_i(\mathbf{x}, t)$  satisfies (3.5).

One can view the macroscopic flow equation (3.6) along with the microscopic evolution equation (3.5) as a coarse-grained model for the original micro-macro model (2.16). To solve the system numerically, it is a natural idea to apply some decoupled schemes at each step. Precisely, we apply the following algorithm for the temporal discretization:

- Step 1: Solve the equation (3.6) by a finite element method to obtain updated values for the velocity and pressure by treating the viscoelastic stress field  $\boldsymbol{\tau}^n$  as a known term obtained from the last time step.
- Step 2: Using the updated velocity field  $\mathbf{u}^{n+1}$ , solve the equation of  $\mathbf{q}_i$ . Update the values of the viscoelastic stress at each node, and project it into the finite element space of  $\boldsymbol{\tau}$ .



In the present work, we adopt the finite element method developed in Ref. 5 and Ref. 16 for the step 1. For more detail, let  $\Omega$  be the bounded computational domain, and  $\mathcal{T}_h$  be the triangulation of  $\Omega$ .  $\mathcal{T}_h$  consists of a set of simplexes  $\{\kappa_e | e = 1, \dots, M\}$  and a set of nodal points  $N_h = \{\mathbf{x}_1, \mathbf{x}_2, \dots, \mathbf{x}_{N_x}\}$ . For a nonnegative integer  $r$ , denote  $P_r(\kappa)$  as the space of polynomial functions of degree less than or equal to  $r$  on the simplex  $\kappa$ . We can construct finite-dimensional subspaces  $S_h \subset H^1(\Omega)$ ,  $M_h \subset L_0^2(\Omega)$  and  $S_h^0 \subset H_0^1(\Omega)$  as follows,

$$S_h = \{g \in C^0(\bar{\Omega}) : g|_{\kappa} \in P_1(\kappa)\}, \quad S_h^0 = \{g \in S_h : g|_{\partial\Omega} = 0\},$$

$$M_h = \{h \in L_0^2(\Omega) : h|_{\kappa} \in P_1(\kappa)\},$$

where  $L_0^2(\Omega) = \{q \in L^2(\Omega), \int_{\Omega} q dx = 0\}$ .

Let the finite element spaces for the velocity and the stress tensor be  $V_{\mathbf{u}_h} = (S_h^0)^d$  and  $V_{\boldsymbol{\tau}} = (S_h)^{d^2}$  respectively, where  $d$  is the dimension of space. Then the equation (3.6) can be solved by a standard velocity-correction projection method.<sup>28</sup> The advantage of using the  $P_1 - P_1$  element for the velocity and pressure is that it avoids an inf-sup condition.<sup>10</sup>

Next we discuss how to solve equation (3.5) with a given flow field  $\mathbf{u}$ . The numerical difficulties arise from the fact that  $\mathbf{q}_i$  is a function of  $\mathbf{x}$  and  $t$  due to the convection term  $\mathbf{u} \cdot \nabla \mathbf{q}_i(\mathbf{x}, t)$ . Many earlier numerical studies based on CONFFESSIT algorithms either focus on the shear flows in which the convection term vanishes or ignore the convection term.<sup>36,57</sup> To deal with the convection term in stochastic methods, there are two types of methods have been developed. One is to introduce a spatial-temporal discretization to  $\mathbf{q}_i$ , as used in Brownian configuration field method.<sup>21,58,70</sup> Another way is to use a Lagrangian viewpoint to compute the convection term.<sup>29</sup> In the current study, we use the idea of the second approach, and use an operator splitting approach to solve (3.5). Initially, we assign ensemble of particles  $\{\mathbf{q}_{\mathbf{x}_{\alpha}, i}\}_{i=1}^N$  to each node  $\mathbf{x}_{\alpha}$  ( $\alpha = 1, 2, \dots, N_x$ ). We assume that  $f(\mathbf{x}, \mathbf{q}, 0)$  is spatially homogenous, and use the same ensemble of initial samples at all  $\mathbf{x}_{\alpha}$ . Within the value  $\mathbf{u}_h^{n+1}$ , we solve the microscopic equation (3.5) by the following two steps:

**Step 1:** At each node  $\mathbf{x}_{\alpha}$ , solve (3.5) without the convection term  $\mathbf{u}^{n+1} \cdot \nabla \mathbf{q}$  by

$$\frac{1}{N} \frac{\mathbf{q}_i^{n+1,*} - \mathbf{q}_i^n}{\Delta t} = -\frac{\delta \mathcal{F}_h}{\delta \mathbf{q}_i}(\{\mathbf{q}_i^{n+1,*}\}_{i=1}^N),$$

$$\mathbf{q}^{n+1,**} = (I + (\nabla \mathbf{u}^{n+1}) \Delta t) \mathbf{q}^{n+1,*}.$$
(3.7)

**Step 2:** To deal with the convention term, we view each node  $\mathbf{x}_{\alpha}$  as an Lagrangian particle, and update it according to the Eulerian velocity field  $\mathbf{u}^{n+1}$  at each node

$$\tilde{\mathbf{x}}_{\alpha} = \mathbf{x}_{\alpha} + \Delta t (\mathbf{u}^{n+1}|_{\mathbf{x}_{\alpha}}), \quad \alpha = 1, 2, \dots, N_x.$$
(3.8)

Hence, the  $\{\mathbf{q}_{\alpha, i}^{n+1,**}\}$  is an ensemble of samples in the new point  $\tilde{\mathbf{x}}_{\alpha}$ . To obtain the  $\mathbf{q}_{\alpha, i}^{n+1}$  at  $\mathbf{x}_{\alpha}$ , we use some interpolation to get  $\mathbf{q}_{\alpha, i}^{n+1}$  (at mesh with  $\{\mathbf{x}_{\alpha}\}$  being the

set of node) from  $\mathbf{q}_{\alpha,i}^{n+1,**}$  (at mesh with  $\{\tilde{\mathbf{x}}_\alpha\}$  being node) for each  $i$ .

**Remark 3.2.** An advantage of the above update-and-projection approach is that it doesn't require a spatial discretization on  $q_i(\mathbf{x}, t)$ .

**Remark 3.3.** The operator splitting approach has been widely used in many previous Fokker-Planck based numerical approaches.<sup>30</sup> One important reason is that the system admits a variational structure without the convention terms. In addition, by treating the convention part separately, we treat the particles at each physical location independently, which largely saves the computational cost.

Since the first step in (3.7) admits a variational structure, the implicit Euler discretization can be reformulated as an optimization problem. In more detail, we define

$$J_n(\{\mathbf{q}_i\}_{i=1}^N) = \frac{1}{N} \sum_{i=1}^N \left( \frac{1}{2\Delta t} |\mathbf{q}_i - \mathbf{q}_i^n|^2 \right) + \mathcal{F}_h.$$

In this case, the first step of (3.7) is the gradient of  $J_n(\{\mathbf{q}_i\}_{i=1}^N)$  with respect to  $\{\mathbf{q}_i\}_{i=1}^N$ . Hence, we can solve the nonlinear system by solving the optimization problem

$$\{\mathbf{q}_i^{n+1,*}\}_{i=1}^N = \arg \min_{\{\mathbf{q}_i\}_{i=1}^N} J_n(\{\mathbf{q}_i\}_{i=1}^N). \quad (3.9)$$

An advantage of this reformulation is that we can prove the existence of the  $\mathbf{q}_i^{n+1,*}$ . More precisely, we have the following result.

**Proposition 3.1.** *For any given  $\{\mathbf{q}_i^n\}_{i=1}^N$ , there exists at least one minimal solution of (3.9)  $\{\mathbf{q}_i^{n+1}\}_{i=1}^N$  that also satisfies*

$$\frac{\mathcal{F}_h(\{\mathbf{q}_i^{n+1}\}_{i=1}^N) - \mathcal{F}_h(\{\mathbf{q}_i^n\}_{i=1}^N)}{\Delta t} \leq -\frac{1}{2N\Delta t^2} \sum_{i=1}^N |\mathbf{q}_i^{n+1} - \mathbf{q}_i^n|^2. \quad (3.10)$$

Moreover, when the velocity  $\mathbf{u} = 0$ , then  $\{\mathbf{q}_i^n\}_{i=1}^N$  converges to a stationary point of  $\mathcal{F}_h$  as  $n \rightarrow \infty$ .

**Proof.** In the case of  $\mathbf{u} = 0$ ,  $\mathcal{F}_h(\{\mathbf{q}_i\}_{i=1}^N)$  is reduced to

$$\mathcal{F}_h(\{\mathbf{q}_i\}_{i=1}^N) = \int_{\Omega} \lambda_p \frac{1}{N} \sum_{i=1}^N \left[ k_B T \ln \left( \frac{1}{N} \sum_{j=1}^N K_h(\mathbf{q}_i - \mathbf{q}_j) \right) + \Psi(\mathbf{q}_i) \right] d\mathbf{x}. \quad (3.11)$$

Let  $\mathbf{X} \in \mathbb{R}^D$  ( $D = N \times d$ ) be vectorized  $\{\mathbf{q}_i\}_{i=1}^N$ , namely,  $\mathbf{X} = (q_{1,1}, \dots, q_{N,1}, q_{1,2}, \dots, q_{N,2}, \dots, q_{N,d})$ . Denote  $\mathcal{F}_h(\{\mathbf{q}_i\}_{i=1}^N)$  and  $J_n(\{\mathbf{q}_i\}_{i=1}^N)$  as  $\mathcal{F}_h(\mathbf{X})$  and  $J_n(\mathbf{X})$  respectively. For given  $\mathbf{X}^n = \{\mathbf{q}_i^n\}_{i=1}^N$ , we define

$$S = \{J_n(\mathbf{X}) \leq J_n(\mathbf{X}^n)\}$$

be the admissible set. Obviously,  $S$  is non-empty and closed, since  $\mathbf{X}^n \in S$  and  $J_n(\mathbf{X})$  is continuous. Moreover, it's easy to prove that  $\mathcal{F}_h(\mathbf{X})$  is bounded from below, since

$$\ln \left( \frac{1}{N} \sum_{j=1}^N K_h(\mathbf{q}_i^n, \mathbf{q}_j^n) \right) \geq \ln \left( \frac{1}{N} \frac{1}{(\sqrt{2\pi}h)^d} \right) \quad \text{and} \quad \Psi(\mathbf{q}_i) \geq 0.$$

And thus,  $J_n(\mathbf{X})$  is coercive and  $S$  is a bounded set. Hence,  $J_n(\mathbf{X})$  admits a global minimizer  $\mathbf{X}^{n+1}$  in  $S$ . Since  $\mathbf{X}^{n+1}$  is a global minimizer of  $J_n(\mathbf{X})$ , we have

$$\frac{1}{N} \sum_{i=1}^N \left( \frac{1}{2\Delta t} |\mathbf{q}_i^{n+1} - \mathbf{q}_i^n|^2 \right) + \mathcal{F}_h(\mathbf{X}^{n+1}) \leq \mathcal{F}_h(\mathbf{X}^n), \quad (3.12)$$

which is equivalent to Eq. (3.10). For the series  $\{\mathbf{q}_i^n\}_{i=1}^N$ , we obtain

$$\frac{1}{N} \sum_{i=1}^N (|\mathbf{q}_i^{k+1} - \mathbf{q}_i^k|^2) \leq 2\Delta t (\mathcal{F}_h(\mathbf{X}^k) - \mathcal{F}_h(\mathbf{X}^{k+1})). \quad (3.13)$$

Summing from 0 to  $n-1$ , we have

$$\frac{1}{N} \sum_{k=0}^{n-1} \sum_{i=1}^N (|\mathbf{q}_i^{k+1} - \mathbf{q}_i^k|^2) \leq 2\Delta t (\mathcal{F}_h(\mathbf{X}^0) - \mathcal{F}_h(\mathbf{X}^n)) \leq C,$$

where  $C$  is some constant independent of  $n$ . Hence,

$$\lim_{n \rightarrow \infty} \frac{1}{N} \sum_{i=1}^N (|\mathbf{q}_i^{n+1} - \mathbf{q}_i^n|^2) = 0,$$

indicating the convergence of  $\{\mathbf{q}_i^n\}_{i=1}^N$ . Moreover, due to Eq. (3.7):

$$\mathbf{q}_i^{n+1} - \mathbf{q}_i^n = -N\Delta t \frac{\delta \mathcal{F}_h}{\delta \mathbf{q}_i}(\{\mathbf{q}_i^{n+1}\}_{i=1}^N),$$

we have

$$\lim_{n \rightarrow \infty} \frac{\delta \mathcal{F}_h}{\delta \mathbf{q}_i}(\{\mathbf{q}_i^n\}_{i=1}^N) = 0.$$

And thus,  $\{\mathbf{q}_i^n\}_{i=1}^N$  converges to a stationary point of  $\mathcal{F}_h$  as  $n \rightarrow \infty$ .  $\square$

The full discretization scheme can be summarized as follows. Given the time step size  $\Delta t$ , the initial conditions  $\{\mathbf{q}_{\alpha,i}^0\}_{i=1}^N$ ,  $\mathbf{u}^0 \in V_{\mathbf{u}_h}$ , and  $p^0 \in M_h$ , having computed for  $\{\mathbf{q}_i^n\}_{i=1}^N$ ,  $\mathbf{u}^n \in V_{\mathbf{u}_h}$ ,  $\boldsymbol{\tau}^n \in V_{\boldsymbol{\tau}}$  and  $p^n \in M_h$  for  $n > 0$ , we compute  $\{\mathbf{q}_i^{n+1}\}_{i=1}^N$ ,  $\mathbf{u}^{n+1}$ , and  $p^{n+1}$  by the following algorithm:

**Step 1:** Treat the stress tensor explicitly and solve the macroscopic flow equation

$$\begin{aligned} \rho \left( \frac{\mathbf{u}^{n+1} - \mathbf{u}^n}{\Delta t} + \mathbf{u}^n \cdot \nabla \mathbf{u}^{n+1} \right) + \nabla p^{n+1} &= \eta_s \Delta \mathbf{u}^{n+1} + \nabla \cdot \boldsymbol{\tau}^n, \\ \nabla \cdot \mathbf{u}^{n+1} &= 0. \end{aligned} \quad (3.14)$$

The equation (3.14) can be solved by the following two steps:

- Step 1.1: Find  $\tilde{\mathbf{u}}_h^{n+1} \in V_{\mathbf{u}_h}$ , such that for any  $\mathbf{v} \in V_{\mathbf{u}_h}$ ,

$$\rho \left( \frac{1}{\Delta t} \tilde{\mathbf{u}}_h^{n+1} + \mathbf{u}_h^n \cdot \nabla \tilde{\mathbf{u}}_h^{n+1}, \mathbf{v} \right) + (\eta_s \nabla \tilde{\mathbf{u}}_h^{n+1}, \nabla \mathbf{v}) = \rho \left( \frac{1}{\Delta t} \mathbf{u}_h^n, \mathbf{v} \right) - (\nabla p_h^n, \mathbf{v}) + (\nabla \cdot \boldsymbol{\tau}_h^n, \mathbf{v}).$$

- Step 1.2: Find  $p_h^{n+1} \in M_h$ , such that for any  $\psi \in M_h$ ,

$$(\nabla(p_h^{n+1} - p_h^n), \nabla \psi) = -\frac{1}{\Delta t} (\nabla \cdot \tilde{\mathbf{u}}_h^{n+1}, \psi).$$

Then we obtain

$$\mathbf{u}_h^{n+1} = \tilde{\mathbf{u}}_h^{n+1} - \Delta t \nabla(p_h^{n+1} - p_h^n).$$

**Step 2:** Within the value  $\mathbf{u}_h^{n+1}$ , we solve the microscopic equation (3.5) by the update-and-project approach. Within the ensemble of particles  $\{\mathbf{q}_{\mathbf{x}_\alpha, i}^{n+1}\}_{i=1}^N$  on each node  $\mathbf{x}_\alpha$ , the updated values of the viscoelastic stress  $\boldsymbol{\tau}^{n+1}$  at each node, denoted as  $\{\boldsymbol{\tau}_{\mathbf{x}_\alpha}^{n+1}\}_{\alpha=1}^{N_x}$ , can be obtained through the second equation of Eq. (3.6). And then project them into the finite element space of  $\boldsymbol{\tau}$ , i.e.  $V_{\boldsymbol{\tau}}$ . To this end, we choose the projection operator  $\mathcal{I}$ , such that, for each component of the stress  $\tau_{\mathbf{x}_\alpha, l, k}^{n+1}$  with  $l, k = 1, \dots, d$ ,  $\mathcal{I}(\{\tau_{\mathbf{x}_\alpha, l, k}^{n+1}\}_{\alpha=1}^{N_x}) := \sum_{\alpha=1}^{N_x} \tau_{\mathbf{x}_\alpha, l, k}^{n+1} \phi_{\mathbf{x}_\alpha}$ , where  $\{\phi_{\mathbf{x}_\alpha} : \alpha = 1, \dots, N_x\} \subset S_h$  denotes the nodal basis for  $S_h$ .

**Remark 3.4.** In the previous numerical scheme, we estimate the macroscopic stress tensor by taking microscopic distribution function as the empirical measure for the finite number of particles  $\{\mathbf{q}_i\}_{i=1}^N$ . More advanced techniques can be applied to this stage to obtain a more accurate estimation to the stress tensor, such as the maximum-entropy based algorithm developed in Ref. 3 and Ref. 61 that reconstructs basis functions from particles. We'll explore this perspective in future works.

## 4. Numerical Experiments

In this section, we perform various numerical experiments to validate the proposed numerical scheme by studying various well-known benchmark problems for the micro-macro models.<sup>32, 42, 57</sup> For all the numerical experiments carried out in this section, we suppose that the flow is two-dimensional and the dumbbells lie in the plane of the flow, namely, the configuration vector  $\mathbf{q}$  is also two-dimensional. At each reach, we use the same initial ensemble of  $N$  particles, sampled from the 2-dimensional standard normal distribution.

### 4.1. Hookean case: the accuracy test

We first consider the Hookean model in a simple shear flow,<sup>12, 42</sup> where the fluid is enclosed between two parallel planes of infinite length separated by a distance

$L$ . At  $t = 0$ , the lower plane starts to move in the positive  $\mathbf{x}$  direction with a constant velocity  $U$ . We consider the no-slip boundary conditions at the walls. In this case, the velocity is in the  $\mathbf{x}$ -direction, and only depends on the  $y$ -variable, namely, the velocity  $\mathbf{u}(\mathbf{x}, t) = (u(y, t), 0)$  with  $\mathbf{x} = (x, y)$ . Obviously, the velocity field automatically satisfies the incompressible condition  $\nabla \cdot \mathbf{u} = 0$ . Moreover, we assume that  $\mathbf{q}$  also only depends on  $y$ , so  $\mathbf{u} \cdot \nabla \mathbf{q} = 0$ .

Since the micro-macro model (2.16) with the Hookean potential  $\Psi(\mathbf{q}) = \frac{1}{2}H|\mathbf{q}|^2$  is equivalent to a macroscopic viscoelastic model, the Oldroyd-B model. We can compare the simulation results for the micro-macro model and the corresponding Oldroyd-B model, as an accuracy test for the proposed numerical scheme. In this subsection, we take the parameters as follows,

$$\rho = 1; \quad \eta_s = 1; \quad \zeta = 4; \quad k_B T = 1; \quad \lambda_p = 1; \quad H = 1; \quad \Delta t = 10^{-3}. \quad (4.1)$$

Such parameters might not be physically reasonable, and we use them primarily to illustrate our numerical scheme. When the parameters are set as Eq. (4.1), the corresponding Oldroyd-B model can be written as follows,<sup>36</sup>

$$\begin{cases} \frac{\partial u}{\partial t}(y, t) = \frac{\partial^2 u}{\partial y^2}(y, t) + \frac{\partial \tau_{12}}{\partial y}(y, t), \\ \frac{\partial \tau_{12}}{\partial t}(y, t) + \tau_{12}(y, t) = \frac{\partial u}{\partial y}(y, t). \end{cases} \quad (4.2)$$

Here,  $\tau_{12}$  denotes the  $(x, y)$  component of the stress  $\boldsymbol{\tau}$ . In this work, these equations are solved sequentially in a segregated manner.<sup>24,59</sup> Namely, for  $0 \leq n \leq \tilde{N}$ , having computed  $u^n$  and  $\tau_{12}^n$ , we compute  $u^{n+1}$  and  $\tau_{12}^{n+1}$  as follows,

$$\begin{aligned} \frac{u^{n+1} - u^n}{\Delta t} &= \frac{\partial^2 u^{n+1}}{\partial y^2} + \frac{\partial \tau_{12}^n}{\partial y}, \\ \frac{\tau_{12}^{n+1} - \tau_{12}^n}{\Delta t} + \tau_{12}^{n+1} &= \frac{\partial u^{n+1}}{\partial y}. \end{aligned} \quad (4.3)$$

For the spatial discretization, we use the same finite element method mentioned in Section 3 to simulate the Oldroyd-B model. For both models, we set the number of elements  $M = 40$  and  $\Delta t = 10^{-3}$ . The kernel bandwidth  $h_p = \text{med}^2 / \log N$ ,<sup>51</sup> where  $\text{med}$  is the median of the pairwise distance between the particles  $\{\mathbf{q}_i^n\}_{i=1}^N$ .

We first study the influence of number of particles. Fig. 1(a) presents the time evolution of  $\tau_{12}$  at  $y = 0.5$  with different number of particles ( $N = 50, 100$  and  $200$ ). The lines in Fig. 1(a) stand for the mean values of 10 independent runs, in which we set the same parameters and use different sets of  $N$  particles (sampled from the standard normal distribution). The shaded regions stand for the standard errors. It reveals that when the particle number gets larger, the standard deviations get small and the mean values get close to the results of the Oldroyd-B model. We set  $N = 200$  for all the following numerical experiments,

Fig. 1(b)-(c) show the time evolution of the simulated stress  $\tau_{12}$  and the velocity  $u$  at  $y = 0.25, 0.5$  and  $0.75$  for the micro-macro model (a single trail) and the

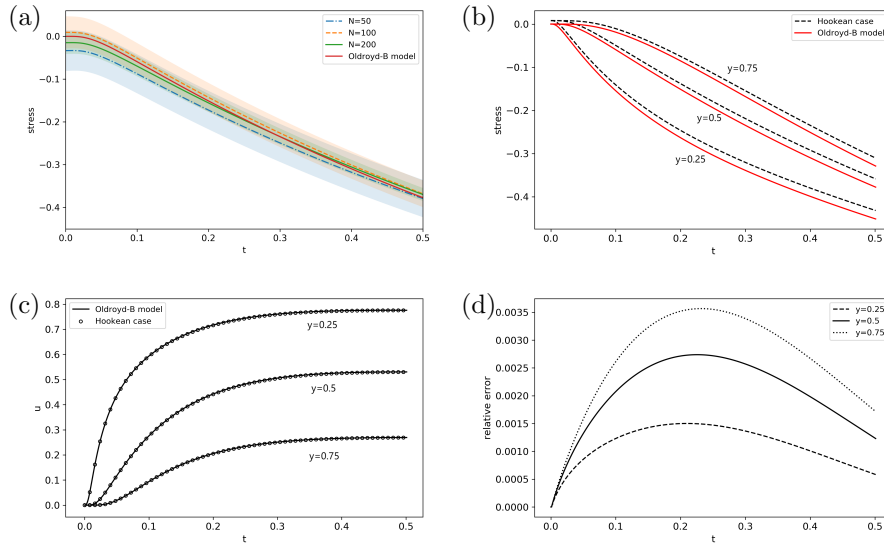


Fig. 1. Time evolution of the stress at  $y = 0.5$  with different numbers of particles (a). Comparison with the Hookean case and the Oldroyd-B model (b-d): the stress with respect to time at different locations (b); comparison of the velocity of the Hookean case (marker) and the Oldroyd-B model (continued line) with respect to time at different locations(c); the relative error of velocity with respect to time at different locations(d).

Oldroyd-B model. Fig. 1(d) shows the relative errors of velocity with respect to time at different locations. The numerical results obtained by the particle scheme are in excellent agreement with numerical results of the Oldroyd-B model, especially for the velocity field, which valid the numerical scheme.

**Remark 4.1.** Since we are mainly interested in the macroscopic flow behavior of the micro-macro model, it is not necessary to solve the microscopic Fokker-Planck equation in high accuracy. The above simulation results indicate that such a simple particle approximation can lead to an accurate estimate to  $\nabla \cdot \boldsymbol{\tau}$ , although a detailed numerical analysis is required to justify this, which will be studied in future works.

#### 4.2. FENE models: Hysteresis behavior in simple extensional flows

The FENE models take the finite extensibility of the polymer chains into account and has nonlinear features. One of the key features of FENE models is hysteresis behavior, which can be observed using the normal stress/the elongational viscosity versus the mean-square extension in simple extensional flow during a relaxation.<sup>20, 45</sup>

In this subsection, we validate our variational particle scheme by studying the hysteresis behavior of a FENE model. We consider an elongational velocity gradient

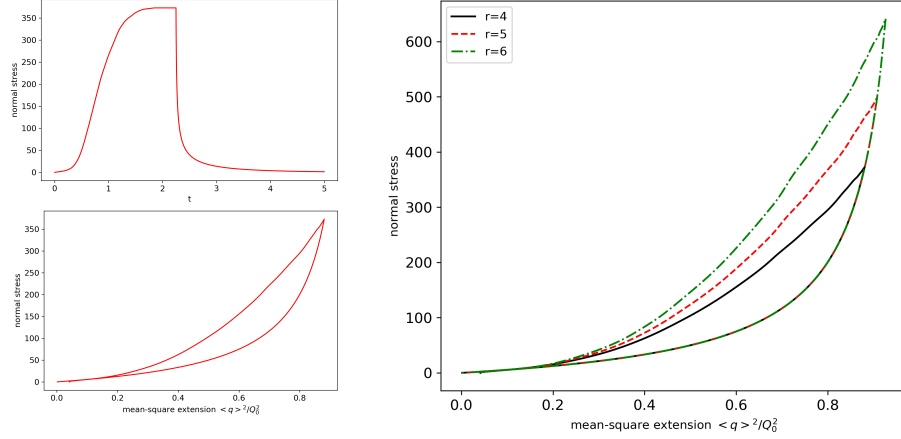


Fig. 2. Left: the start-up case with  $r = 4$ , the time evolution (up) and the hysteresis (bottom) of normal stress  $\tau_{11} - \tau_{22}$ . Right: the hysteresis of the normal stress when  $r = 4, 5$  and  $6$ .

is given by

$$\nabla \mathbf{u} = \varepsilon(t) \text{diag}(1, -1), \quad (4.4)$$

where  $\varepsilon(t)$  is the strain rate and  $\text{diag}(1, -1)$  is the  $2 \times 2$  diagonal matrix with diagonal entries being 1 and  $-1$ . Two cases of  $\varepsilon(t)$  will be considered, the start-up case with

$$\varepsilon(t) = \begin{cases} r & 0 \leq t \leq \frac{9}{r}, \\ 0 & \text{otherwise,} \end{cases} \quad (4.5)$$

and the constant-gradient velocity case with

$$\varepsilon(t) = r. \quad (4.6)$$

Throughout this subsection, the initial data of particles is sampled from the 2-dimensional standard normal distribution and other parameters are set as follows,

$$h_p = 0.01; \quad \zeta = 4; \quad k_B T = 1; \quad \lambda_p = 1; \quad Q_0 = \sqrt{50}; \quad H = 1; \quad \Delta t = 10^{-3}.$$

As stated in Section 4.1, we set  $h_p = \text{med}^2 / \log N$  for Hookean models, where med is the median of the pairwise distance between the particles  $\{\mathbf{q}_i^n\}_{i=1}^N$ . However, this approach is not suitable for the FENE potential, as the equilibrium distributions are no longer Gaussian type and the median of the pairwise distance can become very large. Numerical experiments show that taking  $h_p = 0.01$  produces a good result. Hence, for all the numerical experiments of the FENE case below, we set the kernel bandwidth  $h_p = 0.01$ .

For the start-up case, the numerical results are shown in Figs. 2 and 3 for different extensional rates. The time evolution of normal stress  $\tau_{11} - \tau_{22}$  and the

plot of the normal stress versus the mean-square extension  $\langle q^2 \rangle / Q_0^2$  in the start-up case are plotted in Fig. 2 (left). The comparison of hysteresis behavior of the FENE model for different extensional rates ( $r = 4, 5, 6$ ) is shown in Fig. 2 (right). It is observed that when the strength of velocity gradient is getting smaller, the hysteretic behavior becomes narrow. The numerical results are consistent with those obtained in the former work.<sup>32</sup>

As discussed in Ref. 32, to catch the hysteresis of the original FENE model, a coarse grained model should be able to catch the spike like behaviors of the probability density in the FENE model in large extensional effect of flow field. The peak positions of the probability distribution function (PDF) distribution of the FENE model depend on the macroscopic flow field and change in time under the

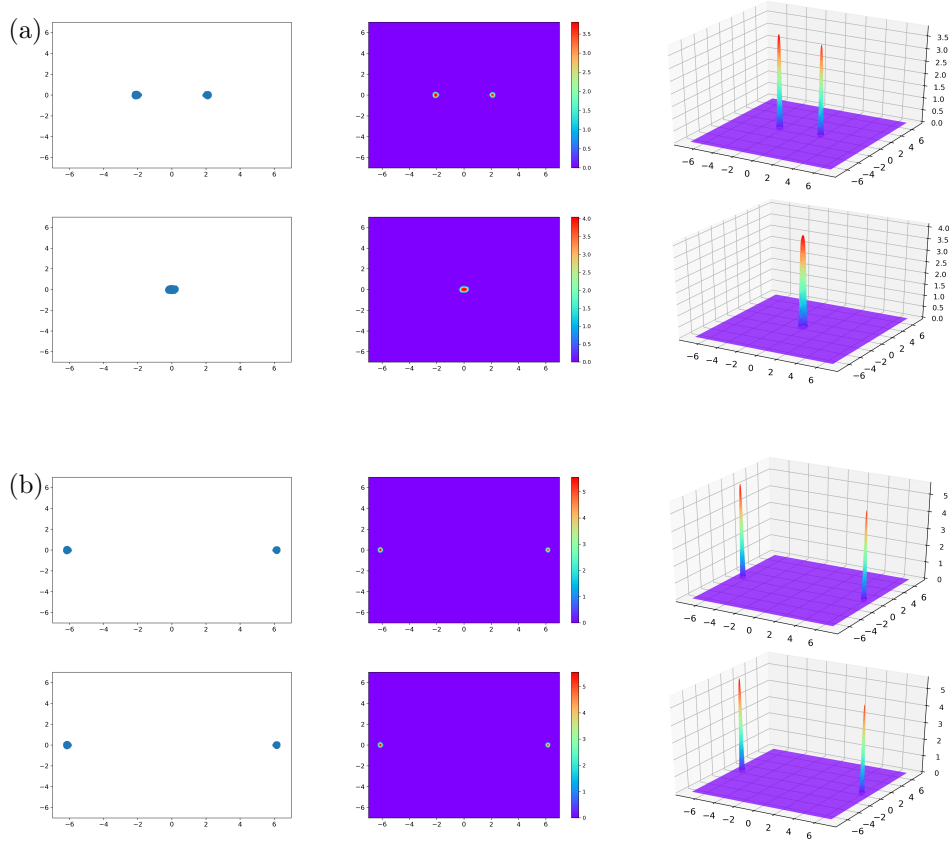


Fig. 3. The particle and corresponding PDF (obtained by kernel density estimation) at different times. (a) Start-up case with  $r = 4$ : the position of particles (left) and the distribution of particles (middle and right) at  $t = 3$  (the first row) and  $t = 8$  (the second row). (b) The constant-gradient velocity case with  $r = 4$ : the position of particles (left) and the distribution of particles (middle and right) at  $t = 3$  (the first row) and  $t = 8$  (the second row).



large macroscopic flow effects.<sup>34</sup> Fig. 3 shows the distribution of the particles (up to a constant) obtained by the kernel density estimation at different times in the start-up case and the constant-gradient velocity case with  $r = 4$ , respectively. It reveals that the distribution of particles captures the  $\delta$ -function like spikes and the time evolution results of the particles apparently show a separation into two peaks in the two cases.

In the start-up case, the distribution splits into two spikes and then shows gradual centralized behavior. Eventually, it forms a single peak in the center, as shown in Fig. 3 (a). Notice that the numerical results in the equilibrium state are consistent with the equilibrium solution of the Fokker-Planck equation with zero flow rate. We can conclude that our numerical results are reasonable, since the velocity rate turns to be zero when  $t$  is big enough ( $t > 9/r$ ). In the constant-gradient velocity case, the particles show two regions of higher concentration near the boundary of the configuration domain at the equilibrium state (i.e., with stable double spikes), as shown in Fig. 3 (b). This is a good agreement to the feature of the FENE model.

It has been well-known that, for the FENE model, there exists several closure approximation approaches to obtain the corresponding macroscopic closure systems, such as FENE-P, FENE-S and FENE-D.<sup>20,32,45,64</sup> Even though some macroscopic closure models show good agreement to macroscopic induced stresses, they are not able to catch the hysteresis and  $\delta$ -function behaviors.<sup>32,64</sup> From the numerical results shown in this section, we could conclude that the variational particle scheme can catch the hysteretic and peak phenomenon, showing good agreement to track the dynamic behaviors of FENE dumbbells.

#### 4.3. FENE case: the pure shear flow

In this section, we consider the case with the FENE potential in the simple shear flow as stated in Section 4.1, where the microscopic particle equations are coupled with the incompressible Navier-Stokes equation on the macroscopic level. In this case, we set  $L = 1$ ,  $M = 20$ ,  $\Delta t = 10^{-3}$  and the same boundary conditions as those in Section 2. The parameters are set as those in Ref. 42:

$$\rho = 1.2757; \eta_s = 0.0521; \zeta = 2; k_B T = 1; H = 0.01; \lambda_p = 1.91; Q_0 = \sqrt{50}. \quad (4.7)$$

Fig. 4 (a) presents the evolution of the velocity with respect to location  $y$  at different times. It reveals the phenomenon of velocity overshoot for the FENE model, which is the typical property of viscoelastic fluids. Fig. 4 (b) displays the evolution of the velocity with respect to time  $t$  at three locations  $y = 0.2$ ,  $y = 0.5$  and  $y = 0.8$ . It can be seen that the velocity overshoot occurs sooner in fluid layers nearer to the moving plane.

Fig. 4(c-d) show the temporal evolution of the shear stress and the normal stress difference at different locations  $y = 0.2$ ,  $y = 0.5$ ,  $y = 0.8$  and  $y = 1$ . As it can be seen, the stress response is sharper in fluid layers nearer to the moving plane, which is consistent with the behavior of velocity overshoot. We notice that there exists

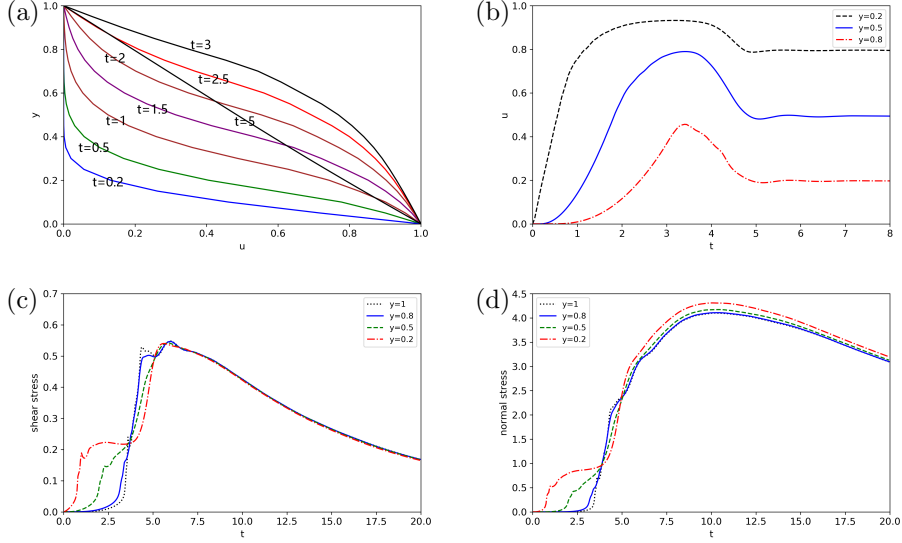


Fig. 4. For the FENE model: the velocity  $u$  with respect to location  $y$  at different times (a); the time evolution of the velocity  $u$  at different locations (b); the time evolution of the shear stress (c) and normal stress difference (d) at location  $y = 0.2$ ,  $y = 0.5$ ,  $y = 0.8$ ,  $y = 1$ .

delay of the maximum of the normal stress with respect to that of the shear stress. Precisely, the shear stress of the FENE model reaches the maximum at around  $t = 6$ , but the maximum of the normal stress is reached at about  $t = 10$ . The numerical results are in excellent agreement with the former work,<sup>42,70</sup> indicating the accuracy of our numerical scheme in the FENE case. Moreover, small oscillations occur in the former work,<sup>70</sup> which is the stochastic noise due to the stochastic nature of the microscopic stress calculation. It should be noted that, compared with the former work, there exists few oscillations in our numerical results obtained by the variational particle scheme.

#### 4.4. FENE models: the lid driven cavity flow

In this section, we consider a more complicated case, known as the lid driven cavity flow. In this case, the polymeric fluid is bounded in a two dimensional square box of width  $L$  and the fluid motion is induced by the translation of the upper wall at a velocity  $U$ . The width of cavity is set to be  $L = 1$  and the velocity  $\mathbf{u} = (u, v)$ , where the horizontal velocity of the lid  $u(x) = U = 1$ . The three other walls are stationary and the boundary conditions applied to them are no slip and impermeability, i.e.,  $\mathbf{u} = \mathbf{0}$ . It is well-known that such idealized lid driven cavity problem possesses a geometric singularity at the edges of the lid. To avoid the numerical difficulty arising from the corner singularity, we consider a regularized boundary condition,<sup>65</sup> given

by

$$u(x) = 16U(x/L)^2(1 - x/L)^2.$$

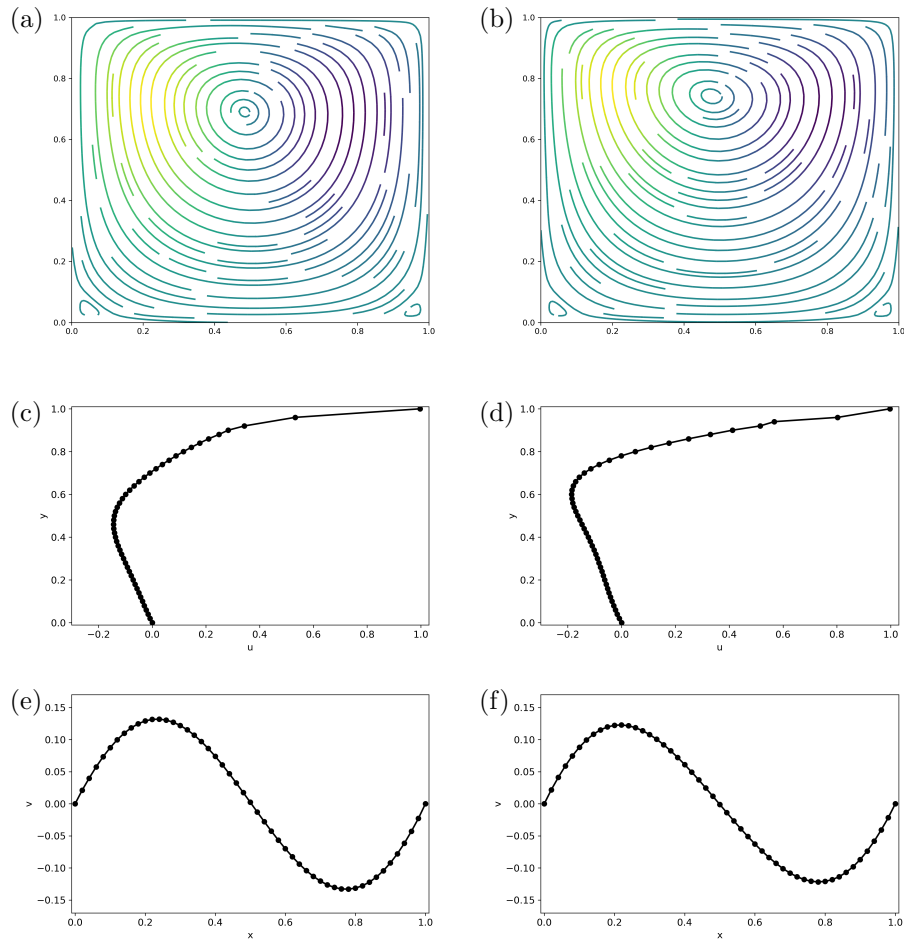


Fig. 5. (a)-(b): The streamlines of the lid driven cavity flow in the FENE case: with  $We = 0.1$  (a) and  $We = 1$  (b). (c)-(d): The profile of  $u$ -velocity on  $x = 0.5$ :  $We = 0.1$  (c) and  $We = 1$  (d). (e)-(f): The profile of  $v$ -velocity on  $y = 0.5$ :  $We = 0.1$  (e) and  $We = 1$  (f).

Since there are no quantitative results for the lid driven cavity flow with FENE dumbbell models, in order to validate our scheme, we make a comparison with the former work,<sup>70</sup> which solves the same model by combining the Brownian configuration field method with an SPH simulation for the macroscopic flow. We consider a

dimensionless version of the micro-macro system Eq. (3.5)-(3.6), which reads

$$\begin{cases} \text{Re}(\mathbf{u}_t + \mathbf{u} \cdot \nabla \mathbf{u}) + \nabla p = \tilde{\eta}_s \Delta \mathbf{u} + \nabla \cdot \boldsymbol{\tau}, \\ \tau = \frac{\epsilon_p}{\text{We}} \frac{1}{N} \sum_{i=1}^N \nabla_{\mathbf{q}} \Psi(\mathbf{q}_i(t)) \otimes \mathbf{q}_i(t), \\ \nabla \cdot \mathbf{u} = 0, \end{cases} \quad (4.8)$$

with  $\mathbf{q}_i(t)$  satisfying

$$\dot{\mathbf{q}}_i - (\nabla \mathbf{u}) \mathbf{q}_i = -\frac{1}{2\text{We}} \left( \frac{\sum_{j=1}^N \nabla_{\mathbf{q}_i} K_h(\mathbf{q}_i, \mathbf{q}_j)}{\sum_{j=1}^N K_h(\mathbf{q}_i, \mathbf{q}_j)} + \sum_{k=1}^N \frac{\nabla_{\mathbf{q}_i} K_h(\mathbf{q}_k, \mathbf{q}_i)}{\sum_{j=1}^N K_h(\mathbf{q}_k, \mathbf{q}_j)} + \nabla_{\mathbf{q}_i} \Psi(\mathbf{q}_i) \right). \quad (4.9)$$

Here, the nondimensionalized parameters are defined as

$$\text{Re} = \frac{\rho \tilde{U} \tilde{L}}{\eta}, \quad \text{We} = \frac{\lambda \tilde{U}}{\tilde{L}}, \quad \tilde{\eta}_s = \frac{\eta_s}{\eta}, \quad \epsilon_p = \frac{\eta_p}{\eta}, \quad \lambda = \frac{\zeta}{4H},$$

where  $\tilde{L} = \sqrt{\frac{k_B T}{H}}$  is the characteristic length scale,  $\tilde{U}$  is the characteristic velocity,  $\eta_p = \lambda_p k_B T \lambda$  is related to the polymer viscosity,  $\eta$  is the total fluid viscosity and  $\eta = \eta_s + \eta_p$ . After the non-dimensionalization, the FENE potential and its gradient become

$$\Psi(\mathbf{q}) = -\frac{b}{2} \ln(1 - |\mathbf{q}|^2/b), \quad \nabla_{\mathbf{q}} \Psi = \frac{\mathbf{q}}{1 - |\mathbf{q}|^2/b},$$

where  $b = H Q_0^2 / k_B T$ .

In numerical experiments, we use a uniform triangular mesh in  $(0, 1) \times (0, 1)$  with  $M = 5000$  and take the time step size  $\Delta t = 10^{-3}$ . Unlike the shear flow cases, the convection term  $\mathbf{u} \cdot \nabla \mathbf{q}$  is non-zero, which is dealt with by a Lagrangian particle approach as introduced in Section 3. Other parameters in the numerical experiments are set as follows:  $\text{Re} = 1$ ;  $\tilde{\eta}_s = 0.11$ ;  $\epsilon_p = 0.889$ ;  $b = \sqrt{50}$ . Fig. 5(a)-(b) show the streamlines for the lid driven cavity flow with  $\text{We} = 0.1$  and  $\text{We} = 1$ , respectively. It is seen that the vortex shifts progressively upward as the  $\text{We}$  number increases. Figs. 5(c)-(d) and 5(e)-(f) describe the u-velocity profile on  $x = 0.5$  and the v-velocity profile on  $y = 0.5$  for the cavity flow with  $\text{We} = 0.1$  and  $\text{We} = 1$ , respectively. The simulation results are consistent with those in the former work,<sup>70</sup> which validate our numerical scheme in the 2D lid driven cavity flow case.

## 5. Conclusion

In this paper, we propose a deterministic particle-FEM discretization to micro-macro models of dilute polymeric fluids. The proposed scheme relies on a coupled numerical solution for the macro- and microscopic scales: a finite element method for the fluid flow equation and a variational particle scheme for the kinetic viscoelastic model. Via a discrete energy variational approach, the derived coarse-grained model of particles preserve the variational structure at the particle level.

The validity of the proposed scheme has been shown through some benchmark problems in the steady flow, shear flow and 2D lid driven cavity flow. The idea can be applied to other complex fluids model, such as the Doi-Onsager model for liquid crystal polymer,<sup>19</sup> the multi-bead spring model<sup>71</sup> and a two species model for wormlike micellar solution,<sup>50,69</sup> which involves a reaction in the microscopic equation.

Although the deterministic particle perform well for current model, it may not be suitable for the multi-bead spring models with a high dimensional Fokker-Planck equation. Another direction for future works is to combine the deterministic particle method with some model reduction techniques, such as the proper orthogonal decomposition (POD) and the proper generalized decomposition (PGD),<sup>17</sup> to reduce the degrees of freedom and therefore the computational cost.

### Acknowledgement

This work is partially supported by the National Science Foundation (USA) grants NSF DMS-1759536, NSF DMS-1950868 (C. Liu, Y. Wang). Part of this work is done when X. Bao visited Department of Applied Mathematics at Illinois Institute of Technology, she would like to acknowledge the hospitality of IIT and the financial support of the China Scholarship Council (No. 201906040019).

### References

1. A. AMMAR, *Lattice boltzmann method for polymer kinetic theory*, J. Non-Newtonian Fluid Mech., 165 (2010), pp. 1082–1092.
2. V. I. ARNOL'D, *Mathematical methods of classical mechanics*, Graduate Texts in Mathematics, 60. Springer-Verlag, New York, 2013.
3. M. ARROYO AND M. ORTIZ, *Local maximum-entropy approximation schemes: a seamless bridge between finite elements and meshfree methods*, Internat. J. Numer. Methods Engrg., 65 (2006), pp. 2167–2202.
4. X. BAO, R. CHEN, AND H. ZHANG, *Constraint-preserving energy-stable scheme for the 2d simplified ericksen-leslie system*, J. Comput. Math., 39 (2021), pp. 1–21.
5. R. BECKER, X. FENG, AND A. PROHL, *Finite element approximations of the ericksen-leslie model for nematic liquid crystal flow*, SIAM J. Numer. Anal., 46 (2008), pp. 1704–1731.
6. V. L. BERDICHEVSKY, *Variational Principles of Continuum Mechanics: I. Fundamentals*, Springer-Verlag, Berlin, 2009.
7. L. BERGAMASCO, S. IZQUIERDO, AND A. AMMAR, *Direct numerical simulation of complex viscoelastic flows via fast lattice-boltzmann solution of the fokker-planck equation*, J. Non-Newtonian Fluid Mech., 201 (2013), pp. 29–38.
8. R. BIRD, C. CURTISS, R. ARMSTRONG, AND O. HASSAGER, *Dynamics of Polymeric Liquids, Kinetic Theory (Dynamics of Polymer Liquids, vol. 1 and 2)*, Wiley-Interscience, New York, 1987.
9. R. B. BIRD AND H. C. OTTINGER, *Transport properties of polymeric liquids*, Annual Review of Physical Chemistry, 43 (1992), pp. 371–406.
10. D. BOFFI, F. BREZZI, AND M. FORTIN, *Mixed Finite Element Methods and Applications*, Springer Series in Computational Mathematics, 44, Springer, Heidelberg, 2013.

11. S. BOYAVAL AND T. LELIÉVRE, *A variance reduction method for parametrized stochastic differential equations using the reduced basis paradigm*, Commun. Math. Sci., 8 (2010), pp. 735–762.
12. C. L. BRIS AND T. LELIÉVRE, *Micro-macro models for viscoelastic fluids: modelling, mathematics and numerics*, Sci. China Math., 55 (2012), pp. 353–384.
13. J. A. CARRILLO, K. CRAIG, AND F. S. PATACCHINI, *A blob method for diffusion*, Calc. Var., 58 (2019), p. 53.
14. C. CHAUVIERE, *A new method for micro-macro simulations of viscoelastic flows*, SIAM J. Sci. Comput., 23 (2002), pp. 2123–2140.
15. C. CHAUVIERE AND A. LOZINSKI, *Simulation of dilute polymer solutions using a fokker-planck equation*, Comput. Fluids, 33 (2004), pp. 687–696.
16. R. CHEN, G. JI, X. YANG, AND H. ZHANG, *Decoupled energy stable schemes for phase-field vesicle membrane model*, J. Comput. Phys., 302 (2015), pp. 509–523.
17. F. CHINESTA, A. AMMAR, A. LEYGUE, AND R. KEUNINGS, *An overview of the proper generalized decomposition with applications in computational rheology*, J. Non-Newtonian Fluid Mech., 166 (2011), pp. 578–592.
18. P. DEGOND AND F.-J. MUSTIELES, *A deterministic approximation of diffusion equations using particles*, SIAM J. Sci. Statist. Comput., 11 (1990), pp. 293–310.
19. M. DOI, S. F. EDWARDS, AND S. F. EDWARDS, *The theory of polymer dynamics*, vol. 73, oxford university press, 1988.
20. P. S. DOYLE, E. S. SHAQFEH, G. H. MCKINLEY, AND S. H. SPIEGELBERG, *Relaxation of dilute polymer solutions following extensional flow*, J. Non-Newtonian Fluid Mech., 76 (1998), pp. 79–110.
21. Q. DU, C. LIU, AND P. YU, *FENE dumbbell model and its several linear and nonlinear closure approximations*, Multiscale Model. Simul., 4 (2005), pp. 709–731.
22. W. E, W. REN, AND E. VANDEN-EIJNDEN, *A general strategy for designing seamless multiscale methods*, Journal of Computational Physics, 228 (2009), pp. 5437–5453.
23. J. L. ERICKSEN, *Reversible and nondissipative processes*, Quart. J. Mech. Appl. Math., 45 (1992), p. 545–554.
24. J. L. FAVERO, A. R. SECCHI, N. S. M. CARDOZO, AND H. JASAK, *Viscoelastic flow analysis using the software openfoam and differential constitutive equations*, J. Non-Newtonian Fluid Mech., 165 (2010), pp. 1625–1636.
25. J. FENG, C. CHAUBAL, AND L. LEAL, *Closure approximations for the doi theory: Which to use in simulating complex flows of liquid-crystalline polymers?*, Journal of Rheology, 42 (1998), pp. 1095–1119.
26. M. GIGA, A. KIRSSTEIN, AND C. LIU, *Variational modeling and complex fluids*, Handbook of mathematical analysis in mechanics of viscous fluids, (2017), pp. 1–41.
27. M. GRIEBEL AND A. RÜTTGERS, *Multiscale simulations of three-dimensional viscoelastic flows in a square-square contraction*, J. Non-Newtonian Fluid Mech., 205 (2014), pp. 42–63.
28. J. L. GUERMOND, P. MINEV, AND J. SHEN, *An overview of projection methods for incompressible flows*, Comput. Methods Appl. Mech. Engrg., 195 (2006), pp. 6011–6045.
29. P. HALIN, G. LIELENS, R. KEUNINGS, AND V. LEGAT, *The lagrangian particle method for macroscopic and micro-macro viscoelastic flow computations*, J. Non-Newtonian Fluid Mech., 79 (1998), pp. 387–403.
30. C. HELZEL AND F. OTTO, *Multiscale simulations for suspensions of rod-like molecules*, J. Comput. Phys., 216 (2006), pp. 52–75.
31. M. A. HULSEN, A. P. G. VAN HEEL, AND B. H. A. A. VAN DEN BRULE, *Simulation of viscoelastic flows using brownian configuration fields*, J. Non-Newtonian Fluid Mech.,

- 70 (1997), pp. 79–101.
32. Y. HYON, *Hysteretic behavior of a moment-closure approximation for fene model*, Kinet. Relat. Mod., 7 (2014), pp. 493–507.
33. Y. HYON, J. A. CARRILLO, Q. DU, AND C. LIU, *A maximum entropy principle based closure method for macro-micro models of polymeric materials*, Kinet. Relat. Models, 1 (2008), pp. 171–184.
34. Y. HYON, Q. DU, AND C. LIU, *An enhanced macroscopic closure approximation to the micro-macro fene model for polymeric materials*, Multiscale Model. Simul., 7 (2008), pp. 978–1002.
35. B. JOURDAIN, C. L. BRIS, AND T. LELIÉVRE, *On a variance reduction technique for micro-macro simulations of polymeric fluids*, J. Non-Newtonian Fluid Mech., 122 (2004), pp. 91–106.
36. B. JOURDAIN, T. LELIÉVRE, AND C. L. BRIS, *Numerical analysis of micro-macro simulations of polymeric fluid flows: a simple case*, Math. Mod. Meth. Appl. S., 12 (2002), pp. 1205–1243.
37. R. KEUNINGS, *On the peterlin approximation for finitely extensible dumbbells*, J. Non-Newtonian Fluid Mech., 68 (1997), pp. 85–100.
38. D. J. KNEZEVIC AND E. SÜLI, *A heterogeneous alternating-direction method for a micro-macro dilute polymeric fluid model*, M2AN Math. Model. Numer. Anal., 43 (2009), pp. 1117–1156.
39. A. P. KOPPOL, R. SURESHKUMAR, AND B. KHOMAMI, *An efficient algorithm for multiscale flow simulation of dilute polymeric solutions using bead-spring chains*, J. Non-Newtonian Fluid Mech., 141 (2007), pp. 180–192.
40. G. LACOMBE AND S. MAS-GALLIC, *Presentation and analysis of a diffusion-velocity method*, in ESAIM: Proc., vol. 7, EDP Sciences, 1999, pp. 225–233.
41. R. LARSON, *The Structure and Rheology of Complex Fluids*, Oxford University Press, Oxford, 1998.
42. M. LASO AND H. C. ÖTTINGER, *Calculation of viscoelastic flow using molecular models: The connffessit approach*, J. Non-Newtonian Fluid Mech., 47 (1993), pp. 1–20.
43. C. LE BRIS AND T. LELIÉVRE, *Micro-macro models for viscoelastic fluids: modelling, mathematics and numerics*, Sci. China Math., 55 (2012), pp. 353–384.
44. T. LI AND P. ZHANG, *Mathematical analysis of multi-scale models of complex fluids*, Commun. Math. Sci., 5 (2007), pp. 1–51.
45. G. LIELENS, P. HALIN, I. JAUMAIN, R. KEUNINGS, AND V. LEGAT, *New closure approximations for the kinetic theory of finitely extensible dumbbells*, J. Non-Newtonian Fluid Mech., 76 (1998), pp. 249–279.
46. F. LIN, *Some analytical issues for elastic complex fluids*, Comm. Pure Appl. Math., 65 (2012), pp. 893–919.
47. F. LIN, C. LIU, AND P. ZHANG, *On a micro-macro model for polymeric fluids near equilibrium*, Comm. Pure Appl. Math., 60 (2007), pp. 838–866.
48. C. LIU, *An introduction of elastic complex fluids: an energetic variational approach*, in Multi-Scale Phenomena in Complex Fluids: Modeling, Analysis and Numerical Simulation, World Scientific, 2009, pp. 286–337.
49. C. LIU AND Y. WANG, *On Lagrangian schemes for porous medium type generalized diffusion equations: A discrete energetic variational approach*, J. Comput. Phys., 417 (2020), p. 109566.
50. C. LIU, Y. WANG, AND T.-F. ZHANG, *Global existence of classical solutions for a reactive polymeric fluid near equilibrium*, arXiv preprint arXiv:2101.11455, (2021).
51. Q. LIU AND D. WANG, *Stein variational gradient descent: A general purpose bayesian inference algorithm*, Advances in Neural Information Processing Systems, 29 (2016).

52. A. LOZINSKI AND C. CHAUVIÈRE, *A fast solver for fokker-planck equation applied to viscoelastic flows calculations: 2d fene model*, J. Comput. Phys., 189 (2003), pp. 607–625.
53. A. LOZINSKI, R. G. OWENS, AND T. N. PHILLIPS, *The langevin and fokker-planck equations in polymer rheology*, in Handbook of numerical analysis, vol. 16, Elsevier, 2011, pp. 211–303.
54. A. LOZINSKI, R. G. OWENS, AND T. N. PHILLIPS, *The langevin and fokker-planck equations in polymer rheology*, Handbook of Numerical Analysis, 16 (2011), pp. 211–303.
55. L. ONSAGER, *Reciprocal relations in irreversible processes. i.*, Phys. Rev., 37 (1931), p. 405.
56. ———, *Reciprocal relations in irreversible processes. ii.*, Phys. Rev., 38 (1931), p. 2265.
57. H. ÖTTINGER, *Stochastic Processes in Polymeric Fluids, Tools and Examples for Developing Simulation Algorithms*, Springer-Verlag, Berlin, 1996.
58. H. C. ÖTTINGER, B. VAN DEN BRULE, AND M. HULSEN, *Brownian configuration fields and variance reduced connffessit*, J. Non-Newtonian Fluid Mech., 70 (1997), pp. 255–261.
59. F. PIMENTA AND M. A. ALVES, *Stabilization of an open-source finite-volume solver for viscoelastic fluid flows*, J. Non-Newtonian Fluid Mech., 239 (2017), pp. 85–104.
60. L. RAYLEIGH, *Some general theorems relating to vibrations*, Proc. Lond. Math. Soc., 1 (1871), pp. 357–368.
61. A. ROSOLEN, C. PECO, AND M. ARROYO, *An adaptive meshfree method for phase-field models of biomembranes. part i: Approximation with maximum-entropy basis functions*, J. Comput. Phys., 249 (2013), pp. 303–319.
62. G. RUSSO, *Deterministic diffusion of particles*, Comm. Pure Appl. Math., 43 (1990), pp. 697–733.
63. J. SHEN AND H. YU, *On the approximation of the fokker-planck equation of the finitely extensible nonlinear elastic dumbbell model i: A new weighted formulation and an optimal spectral-galerkin algorithm in two dimensions*, SIAM J. Numer. Anal., 50 (2012), pp. 1136–1161.
64. R. SIZAIRE, G. LIELENS, I. JAUMAIN, R. KEUNINGS, AND V. LEGAT, *On the hysteretic behaviour of dilute polymer solutions in relaxation following extensional flow*, J. Non-Newtonian Fluid Mech., 82 (1999), pp. 233–253.
65. R. G. SOUSA, R. J. POOLE, A. M. AFONSO, F. T. PINHO, P. J. OLIVEIRA, A. MOROZOV, AND M. A. ALVES, *Lid-driven cavity flow of viscoelastic liquids*, J. Non-Newtonian Fluid Mech., 234 (2016), pp. 129–138.
66. J. K. C. SUEN, Y. L. JOO, AND R. C. ARMSTRONG, *Molecular orientation effects in viscoelasticity*, Annu. Rev. Fluid Mech., 34 (2002), pp. 417–444.
67. Y. WANG, J. CHEN, L. KANG, AND C. LIU, *Particle-based energetic variational inference*, Stat. Comput., 31 (2021), pp. Paper No. 34, 17pp.
68. Y. WANG, C. LIU, P. LIU, AND B. EISENBERG, *Field theory of reaction-diffusion: law of mass action with an energetic variational approach*, Phys. Rev. E, 102 (2020), pp. 062147, 9 pp.
69. Y. WANG, T.-F. ZHANG, AND C. LIU, *A two species micro-macro model of wormlike micellar solutions and its maximum entropy closure approximations: An energetic variational approach*, J. Non-Newtonian Fluid Mech., 293 (2021), p. 104559.
70. X. XU, J. OUYANG, W. LI, AND Q. LIU, *Sph simulations of 2d transient viscoelastic flows using brownian configuration fields*, J. Non-Newtonian Fluid Mech., 208-209 (2014), pp. 59–71.
71. Q. ZHOU AND R. AKHAVAN, *Cost-effective multi-mode fene bead-spring models for*



*dilute polymer solutions*, J. Non-Newtonian Fluid Mech., 116 (2004), pp. 269–300.